

Many-Impurity Effects in Fourier Transform Scanning Tunneling Spectroscopy

O. Kodra and W. A. Atkinson

Department of Physics, Trent University, 1600 West Bank Dr., Peterborough ON, K9J 7B8, Canada

(Dated: November 20, 2018)

Fourier transform scanning tunneling spectroscopy (FTSTS) is a useful technique for extracting details of the momentum-resolved electronic band structure from inhomogeneities in the local density of states due to disorder-related quasiparticle scattering. To a large extent, current understanding of FTSTS is based on models of Friedel oscillations near isolated impurities. Here, a framework for understanding many-impurity effects is developed based on a systematic treatment of the variance $\Delta\rho^2(\mathbf{q}, \omega)$ of the Fourier transformed local density of states $\rho(\mathbf{q}, \omega)$. One important consequence of this work is a demonstration that the poor signal-to-noise ratio inherent in $\rho(\mathbf{q}, \omega)$ due to randomness in impurity positions can be eliminated by configuration averaging $\Delta\rho^2(\mathbf{q}, \omega)$. Furthermore, we develop a diagrammatic perturbation theory for $\Delta\rho^2(\mathbf{q}, \omega)$ and show that an important bulk quantity, the mean-free-path, can be extracted from FTSTS experiments.

I. INTRODUCTION

As a result of technical advances in scanning tunneling microscopy (STM) methods, it has become possible to measure the quasiparticle spectrum at surfaces of a variety of materials over large areas with both atomic spatial resolution and mV energy resolution. While STM is a powerful and direct probe of electronic wavefunctions, the interpretation of STM spectra generally requires comparison with a model spectrum calculated using approximate many-body techniques (for example, the local density approximation). This can be problematic in situations where details of the surface are poorly known, or where traditional theoretical methods fail, as in the high temperature superconductors. The question of how one can usefully analyze STM spectral maps without a detailed quantitative model of the electronic structure is therefore paramount.

Recently, it was shown that details of the quasiparticle dispersion can be extracted from the spatial Fourier transform of STM spectra on disordered surfaces.¹ The technique is often referred to as Fourier transform scanning tunneling spectroscopy (FTSTS) and requires that maps of the local density of states (LDOS) $\rho(\mathbf{r}, \omega)$ at energy ω be made over reasonably large surface areas, from which the Fourier transform, $\rho(\mathbf{q}, \omega) = \sum_{\mathbf{r}} \rho(\mathbf{r}, \omega) \exp(-i\mathbf{q} \cdot \mathbf{r})$, can be obtained. In the simplest case, that of noninteracting quasiparticles, the LDOS at position \mathbf{r} and energy ω is

$$\rho(\mathbf{r}, \omega) = \sum_n |\Psi_n(\mathbf{r})|^2 \delta(\omega - E_n), \quad (1)$$

where $\Psi_n(\mathbf{r})$ is the n^{th} quasiparticle eigenstate with energy E_n . For a clean surface, $\Psi_n(\mathbf{r})$ are Bloch states of the form $\phi_{j,\mathbf{k}}(\mathbf{r})e^{i\mathbf{k} \cdot \mathbf{r}}$ with wavevector \mathbf{k} and band index j , and $\rho(\mathbf{r}, \omega) = \sum_{j,\mathbf{k}} |\phi_{j,\mathbf{k}}(\mathbf{r})|^2 \delta(\omega - E_{j\mathbf{k}})$ has only the spatial periodic modulations of the unit cell. However, in the presence of defects, the eigenstates contain mixtures of Bloch states with different values of \mathbf{k} , and the probability density $|\Psi_n(\mathbf{r})|^2$ exhibits standing wave patterns (Friedel oscillations) arising from the interference between these different \mathbf{k} -values. Near an isolated impurity,

for example, one can decompose the eigenstates at energy ω into initial and final (scattered) states with wavevectors \mathbf{k}_i and \mathbf{k}_f respectively. Then, the Fourier transformed density of states (FTDOS) is peaked at wavevectors $\mathbf{q} = \mathbf{k}_f - \mathbf{k}_i$ for which \mathbf{k}_f and \mathbf{k}_i lie on constant energy contours of energy ω . This is illustrated in Fig. 1: in panel (a) the FTDOS is calculated (details given later) at the Fermi energy $\omega = 0$ for a single impurity in a 2D tight-binding metal whose Fermi surface is shown in panel (b). The arrows \mathbf{q}_1 and \mathbf{q}_2 in (b) label transitions between states on the Fermi surface which contribute to the maxima at \mathbf{q}_1 and \mathbf{q}_2 in (a). There is, therefore, a direct connection between $\rho(\mathbf{q}, \omega)$ and the quasiparticle energy dispersion $\epsilon_{\mathbf{k}}$. The possibility of using FTSTS to map out $\epsilon_{\mathbf{k}}$ was first demonstrated by Sprunger *et al.*¹ and FTSTS has since been used by several groups to study metal surfaces,^{2,3} semiconductors,^{4,5} semimetals,⁶ and strongly-correlated superconductors.^{7,8,9,10} Quite recently, an extension of this technique to study inelastic scattering in strongly-correlated superconductors has been proposed.¹¹

The usefulness of the FTSTS method, however, is limited by the large signal-to-noise ratio which is invariably present. This is an intrinsic problem, as we now illustrate, which arises from the randomness of the impurity positions. We assume, for simplicity, that a random distribution of N_i identical impurities sit at sites \mathbf{R}_i , $i = 1, \dots, N_i$ and that the impurities do not interfere substantially, so that each impurity modifies the LDOS by an amount $\delta\rho(\mathbf{r} - \mathbf{R}_i, \omega)$. This term is meant to describe the Friedel oscillations in the vicinity of an isolated impurity, and its Fourier transform $\delta\rho(\mathbf{q}, \omega)$ is the quantity one wishes to study experimentally. For simplicity, we will ignore sub-unit-cell modulations of the LDOS due to the crystalline potential so that the LDOS is uniform in the absence of impurities. Then, with the impurities present, $\rho(\mathbf{r}, \omega) = \rho_0(\omega) + \sum_{i=1}^{N_i} \delta\rho(\mathbf{r} - \mathbf{R}_i, \omega)$, and it follows that

$$\rho(\mathbf{q}, \omega) = [N\rho_0(\omega) + N_i\delta\rho(\mathbf{q}, \omega)]\delta_{\mathbf{q},0} + \delta\rho(\mathbf{q}, \omega)\sqrt{N_i}f(\mathbf{q}), \quad (2)$$

where $\delta\rho(\mathbf{q}, \omega) = \sum_{\mathbf{r}} e^{-i\mathbf{q} \cdot \mathbf{r}} \delta\rho(\mathbf{r}, \omega)$ is the Fourier trans-

form of the scattering pattern due to a *single* impurity, N is the number of spatial points included in the Fourier transform, and

$$f(\mathbf{q}) = \frac{\delta_{\mathbf{q} \neq 0}}{\sqrt{N_i}} \sum_{i=1}^{N_i} e^{-i\mathbf{q} \cdot \mathbf{R}_i},$$

is a random function of \mathbf{q} normalized such that $|f(\mathbf{q})| \sim 1$ and $\delta_{\mathbf{q} \neq 0} = 1 - \delta_{\mathbf{q},0}$. The form of Eq. (2) was first demonstrated in the limit of weak impurities by Capriotti *et al.*¹² and then for a dilute distribution of pointlike impurities of arbitrary strength by Zhu *et al.*¹³. We make two comments regarding Eq. (2). First, for a *particular* disorder configuration, and for $\mathbf{q} \neq 0$, $\rho(\mathbf{q}, \omega)$ is the product of a useful signal $\delta\rho(\mathbf{q}, \omega)$ and a noise term $f(\mathbf{q})$. In practice, this means that the noise is as large as the signal, and that it can be nearly impossible to resolve the fine details of the FTDOS spectrum which have been predicted in numerous calculations. This is particularly true in the cuprate superconductors, which are inherently dirty materials. This point is illustrated in Fig. 1 where the FTDOS is shown for a 2D metal for both a single point scatterer in panel (a), and a random configuration of 3% impurities in panel (c) (the details of the calculation will be given below). The figure clearly demonstrates the difficulty one faces when dealing with disordered systems; while the FTDOS pattern is visible in (c), one would have difficulty making a quantitative comparison of the structure with (a). The second comment is that in nearly all calculations to date, $\delta\rho(\mathbf{q}, \omega)$ has been calculated in the clean limit, ie. for a single impurity. This approximation captures many qualitative features of the spectrum, but also risks failing when the scattering rate is large, as appears to be the case in the cuprate superconductors. It is natural to assume that disorder, in addition to producing noise, must introduce a quasiparticle scattering rate γ which broadens $\delta\rho(\mathbf{q}, \omega)$, but it is in fact not obvious. Formally, the elastic scattering rate appears when one averages a large number of impurity configurations, and is not defined when one studies a particular configuration of impurities. If, for example, we try to take the disorder average $\langle \rho(\mathbf{q}, \omega) \rangle$, where $\langle \dots \rangle$ indicates a configuration average, we find that since $f(\mathbf{q})$ is a sum of random phases, $\langle f(\mathbf{q}) \rangle = 0$ and

$$\langle \rho(\mathbf{q}, \omega) \rangle = [N\rho_0(\omega) + N_i\delta\rho(\mathbf{q}, \omega)]\delta_{\mathbf{q},0}. \quad (3)$$

In other words, one does not simply find that $\rho(\mathbf{q}, \omega)$ is broadened by disorder, but rather that in the process of configuration averaging $\rho(\mathbf{q}, \omega)$, one loses the finite- \mathbf{q} signal altogether.

It is therefore the goal of this paper to develop a systematic disorder-averaged formalism for understanding many-impurity effects in FTSTS. In Sec. II A, we demonstrate that the variance, $\langle \Delta\rho^2(\mathbf{q}, \omega) \rangle \equiv \langle |\rho(\mathbf{q}, \omega)|^2 \rangle - |\langle \rho(\mathbf{q}, \omega) \rangle|^2$, retains the useful finite- \mathbf{q} information when disorder-averaged, and that the random noise described by $f(\mathbf{q})$ is eliminated as a result of configuration averaging. Results are illustrated with numerical calculations

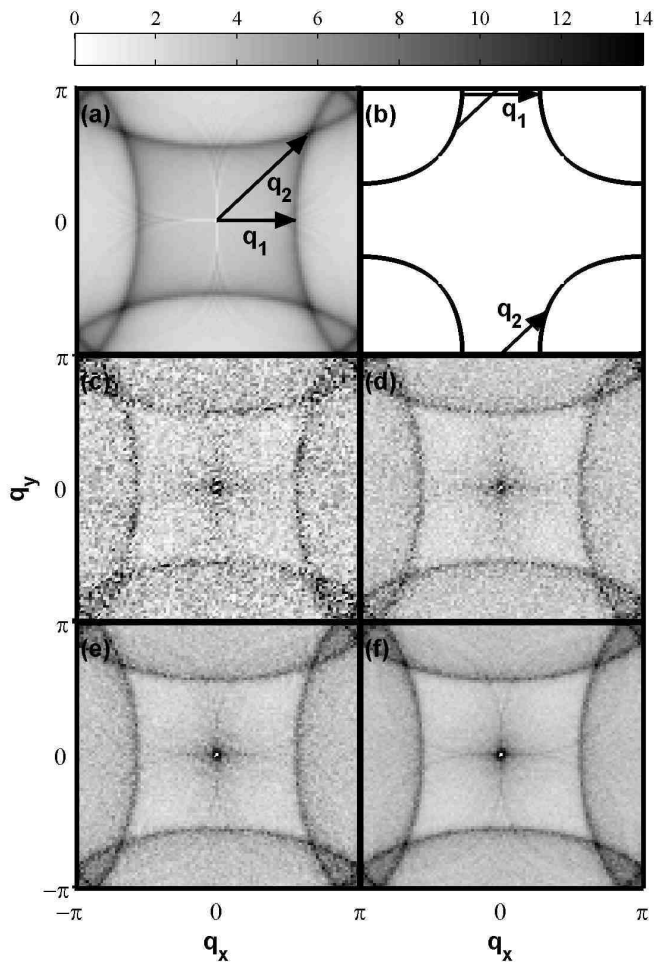


FIG. 1: (color online) Effect of randomness in the impurity distribution on the FTDOS of the 2D tight-binding metal described in Sec. II B. (a) $\rho(\mathbf{q}, \omega)$ is plotted for a single pointlike impurity embedded in a 100×100 lattice. The Fermi surface contour $\epsilon_{\mathbf{k}} = 0$ is shown in (b). Arrows \mathbf{q}_1 and \mathbf{q}_2 show the scattering transitions producing the features labelled \mathbf{q}_1 and \mathbf{q}_2 in (a). The FTDOS for 3% randomly distributed impurities is shown averaged over N_{cfg} configurations for (c) $N_{\text{cfg}} = 1$, (d) $N_{\text{cfg}} = 4$, (e) $N_{\text{cfg}} = 10$, (f) $N_{\text{cfg}} = 29$. In (c), $|\rho(\mathbf{q}, \omega)|$ is plotted, while in (d)-(f), we plot the root-mean-square FTDOS $\rho_{\text{rms}}(\mathbf{q}, \omega) \equiv \sqrt{\langle \Delta\rho^2(\mathbf{q}, \omega) \rangle_{N_{\text{cfg}}}}$. In all figures, we take $\omega = 0$ and an impurity potential of $V = 10t_1$. Other model details are given in Sec. II B.

described in Sec. II B. Finally, we show in Sec. II C that one can develop a diagrammatic perturbation theory for $\langle \Delta\rho^2(\mathbf{q}, \omega) \rangle$ in which many-impurity effects can be understood systematically. One useful consequence of these calculations is a demonstration that the mean free path can be extracted from FTSTS spectra. A summary of these results will be presented in Sec. III.

II. THEORY AND CALCULATIONS

A. Simple Model

For a finite number N_{cfg} of impurity configurations, the variance of the FTDOS is $\langle \Delta\rho^2(\mathbf{q}, \omega) \rangle_{N_{\text{cfg}}} \equiv \langle |\rho(\mathbf{q}, \omega)|^2 \rangle_{N_{\text{cfg}}} - |\langle \rho(\mathbf{q}, \omega) \rangle_{N_{\text{cfg}}}|^2$. We keep N_{cfg} finite for the moment because, in practical applications where it can be time consuming to obtain spectra of the disordered system, one might find that it is only possible to average over a relatively small number of configurations, and it is therefore useful to understand how the noise scales with N_{cfg} . Configuration averaging is performed by averaging over sets of impurity positions denoted by \mathbf{R}_i^n with $n = 1, \dots, N_{\text{cfg}}$ indicating the different configurations, and $i = 1, \dots, N_i$ labelling impurities. We typically need to compute averages of the form

$$\left\langle \sum_{i=1}^{N_i} e^{-i\mathbf{q}\cdot\mathbf{R}_i} \right\rangle_{N_{\text{cfg}}} \equiv \frac{1}{N_{\text{cfg}}} \sum_{n=1}^{N_{\text{cfg}}} \sum_{i=1}^{N_i} e^{-i\mathbf{q}\cdot\mathbf{R}_i^n}.$$

Since, for fixed \mathbf{q} , this is just a random walk in the complex plane with $N_{\text{cfg}}N_i$ steps, it follows that

$$\left\langle \sum_{i=1}^{N_i} e^{-i\mathbf{q}\cdot\mathbf{R}_i} \right\rangle_{N_{\text{cfg}}} = N_i \delta_{\mathbf{q},0} + \sqrt{\frac{N_i}{N_{\text{cfg}}}} f(\mathbf{q}), \quad (4)$$

where, as always, $f(\mathbf{q})$ is a random complex function of \mathbf{q} for $\mathbf{q} \neq 0$ with $|f(\mathbf{q})| \sim O(1)$ and $f(0) = 0$. Using Eqs. (2) and (4), one can show that

$$\begin{aligned} \langle \rho(\mathbf{q}, \omega) \rangle_{N_{\text{cfg}}} &= [N\rho_0(\omega) + N_i \delta\rho(\mathbf{q}, \omega)] \delta_{\mathbf{q},0} \\ &\quad + \delta\rho(\mathbf{q}, \omega) \sqrt{\frac{N_i}{N_{\text{cfg}}}} f(\mathbf{q}), \end{aligned} \quad (5)$$

and that

$$\begin{aligned} \langle |\rho(\mathbf{q}, \omega)|^2 \rangle_{N_{\text{cfg}}} &= [N\rho_0(\omega) + N_i \delta\rho(\mathbf{q}, \omega)]^2 \delta_{\mathbf{q},0} \\ &\quad + N_i |\delta\rho(\mathbf{q}, \omega)|^2 \left[1 + \frac{\text{Re}f(\mathbf{q})}{\sqrt{N_{\text{cfg}}}} \right], \end{aligned} \quad (6)$$

so that

$$\langle \Delta\rho^2(\mathbf{q}, \omega) \rangle_{N_{\text{cfg}}} = N_i |\delta\rho(\mathbf{q}, \omega)|^2 \left[1 + \frac{\text{Re}f(\mathbf{q})}{\sqrt{N_{\text{cfg}}}} \right], \quad (7)$$

to leading order in N_{cfg} . Equation (7) is the principal result for this subsection, and it demonstrates the key ideas of this paper which are that (i) the signal-to-noise ratio of the variance of $\rho(\mathbf{q}, \omega)$ *improves* with configuration averaging and (ii) $\lim_{N_{\text{cfg}} \rightarrow \infty} \langle \Delta\rho^2(\mathbf{q}, \omega) \rangle_{N_{\text{cfg}}}$ is nonvanishing. The latter point suggests that one can construct a disorder-averaged perturbation series for $\langle \Delta\rho^2(\mathbf{q}, \omega) \rangle$, which we will do in Sec. II C.

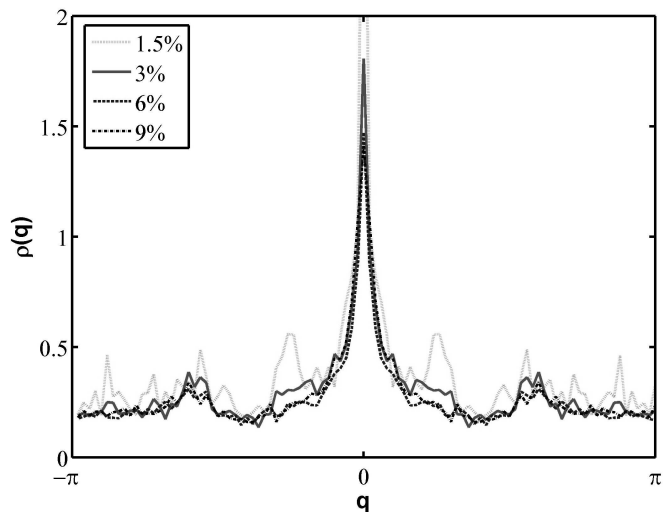


FIG. 2: (color online) Scaling of FTDOS with number of impurities. Cuts of $\rho_{\text{rms}}(\mathbf{q}, \omega)/\sqrt{N_i}$ along $\mathbf{q} = (q, 0)$ are shown for different impurity concentrations and for $N_{\text{cfg}} = 29$, $\omega = 0$.

B. Numerical Method

In order to illustrate the results of the previous section, and to compare with the diagrammatic perturbation series presented in the next section, we have calculated the FTDOS exactly for noninteracting quasiparticles in a disordered 2D metal. For simplicity, we take pointlike disorder and a tight-binding band structure of the form

$$\epsilon_{\mathbf{k}} = t_0 - 2t_1(\cos k_x + \cos k_y) + 4t_2 \cos k_x \cos k_y.$$

This band structure is often used to describe high temperature superconductors, but is chosen primarily because it is amenable to the real-space numerical method described here. For concreteness, we measure energies in units of t_1 and take $t_0 = 0.5t_1$ and $t_2 = 0.45t_1$. The Fermi surface for this band structure is shown in Fig. 1(b).

In real space, the Hamiltonian is defined on a square lattice

$$\hat{H} = \sum_{i,j} \sum_{\sigma} t_{ij} c_{\mathbf{r}_i\sigma}^{\dagger} c_{\mathbf{r}_j\sigma} + V_0 \sum_{\ell=1}^{N_i} \sum_{\sigma} c_{\mathbf{R}_{\ell}\sigma}^{\dagger} c_{\mathbf{R}_{\ell}\sigma} \quad (8)$$

where $c_{\mathbf{r},\sigma}$ is the annihilation operator for a quasiparticle on site i with spin σ , and $t_{ii} = t_0$, $t_{ij} = -t_1$ for i and j nearest neighbor sites, and $t_{ij} = t_2$ for next-nearest-neighbor sites. As before, \mathbf{R}_{ℓ} are the impurity site locations, and the impurities have strength $V_0 = 10t_1$. Equation (8) can be diagonalized numerically, and the eigenenergies E_n and eigenvectors $\Psi_n(\mathbf{r}_i)$ can be inserted into Eq. (1) to find $\rho(\mathbf{r}, \omega)$, from which $\Delta\rho^2(\mathbf{q}, \omega)$ follows directly. We remark that for simulations in which $N_{\text{cfg}} = 1$, we plot $|\rho(\mathbf{q}, \omega)|$, while for $N_{\text{cfg}} > 1$, we actually plot the root-mean-square variance

$$\rho_{\text{rms}}(\mathbf{q}, \omega) \equiv \sqrt{\langle \Delta\rho^2(\mathbf{q}, \omega) \rangle_{N_{\text{cfg}}}},$$

which is most the most natural quantity to compare with $|\rho(\mathbf{q}, \omega)|$.

The numerical approach adopted here restricts the system size to $\lesssim 10000$ lattice sites, and other methods¹⁴ exist which allow one to study larger systems in the dilute impurity limit. However, in many interesting situations (eg. ones in which interactions are important) numerical calculations will be similarly restricted. This system size is also comparable to typical surface areas studied in FTSTS experiments. In general, one can expect the FTDOS to be consistent with the predictions of the perturbation theory introduced below provided the system is larger than the mean-free path.

The scaling with N_i and N_{cfg} suggested by Eq. (7) has been tested numerically using the method outlined in this section and holds for a wide range of impurity concentrations, as shown in Fig. 1 and Fig. 2. In Fig. 1, one sees that an average over only four configurations improves the signal-to-noise ratio significantly (by about a factor of 2) and that fine details of the FTDOS can be resolved when one averages over ≈ 10 configurations. One also sees in Fig. 2 that the spectrum generally scales as $\sqrt{N_i}$ as expected. Closer inspection reveals that most of the peaks evident at smaller impurity concentrations are due to finite size effects and disappear at larger concentrations where the mean-free-path is less than the system size. Furthermore, the peak at $\mathbf{q} \approx (1.9, 0)$, corresponding to \mathbf{q}_1 in Fig. 1, deviates from the simple scaling at smaller values of N_i , but satisfies the $\sqrt{N_i}$ -scaling relation best when the mean-free-path is less than the system size.

C. Diagrammatic Method

The goal of this section is to develop a diagrammatic perturbation series for $\langle \Delta \rho^2(\mathbf{q}, \omega) \rangle$. The LDOS is defined in terms of single-particle Green's functions as

$$\rho(\mathbf{r}, \omega) = -\frac{1}{2\pi i} [\mathcal{G}^+(\mathbf{r}, \mathbf{r}, \omega) - \mathcal{G}^-(\mathbf{r}, \mathbf{r}, \omega)],$$

where \mathcal{G}^+ and \mathcal{G}^- are the retarded and advanced Green's functions for a *particular* disorder configuration. Then we can write,

$$\begin{aligned} |\rho(\mathbf{q}, \omega)|^2 &= \frac{-1}{(2\pi)^2} \sum_{s_1, s_2 = \pm} s_1 s_2 \sum_{\mathbf{r}_1, \mathbf{r}_2} e^{-i\mathbf{q} \cdot \mathbf{r}_{12}} \\ &\quad \times \mathcal{G}^{s_1}(\mathbf{r}_1, \mathbf{r}_1, \omega) \mathcal{G}^{s_2}(\mathbf{r}_2, \mathbf{r}_2, \omega), \\ &= \frac{-1}{(2\pi)^2} \sum_{s_1, s_2 = \pm} s_1 s_2 \sum_{\mathbf{k}_1, \mathbf{k}_2} \\ &\quad \times \mathcal{G}^{s_1}(\mathbf{k}_1, \mathbf{k}_1 - \mathbf{q}, \omega) \mathcal{G}^{s_2}(\mathbf{k}_2, \mathbf{k}_2 + \mathbf{q}, \omega), \end{aligned}$$

where $\mathbf{r}_{12} = \mathbf{r}_1 - \mathbf{r}_2$. The disorder average of \mathcal{G}^\pm is

$$\langle \mathcal{G}^\pm(\mathbf{k}, \mathbf{k} + \mathbf{q}, \omega) \rangle = G^\pm(\mathbf{k}, \omega) \delta_{\mathbf{q}, 0},$$

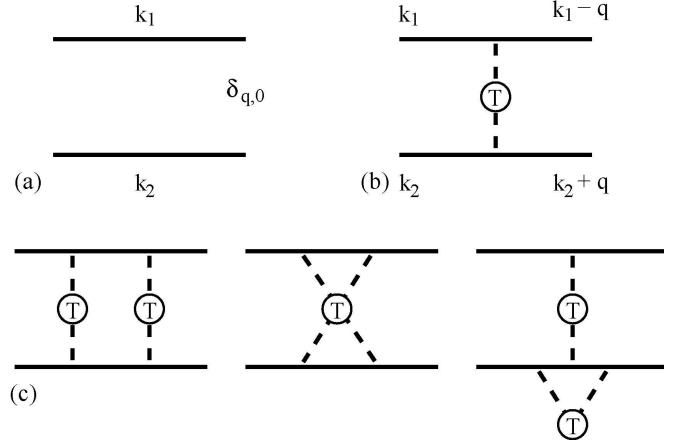


FIG. 3: Diagrams relevant to the calculation of $\langle \Delta \rho^2(\mathbf{q}, \omega) \rangle$. (a) Disconnected diagrams cancel in the difference $\langle |\rho(\mathbf{q}, \omega)|^2 \rangle - |\langle \rho(\mathbf{q}, \omega) \rangle|^2$. (b) Leading order and (c) second order diagrams which are computed in the text. In all diagrams, solid lines represent fully self-consistent Green's functions (retarded or advanced) and each pair of dashed lines connecting to a vertex labelled "T" represents $n_i T^\pm(\omega) T^\pm(\omega)$.

where $G(\mathbf{k}, \omega)$ is the usual self-consistent disorder-averaged Green's function. It follows that

$$\begin{aligned} \langle |\rho(\mathbf{q}, \omega)|^2 \rangle &= \left[\frac{1}{2\pi} \sum_{s, \mathbf{k}} s \mathbf{G}^s(\mathbf{k}, \omega) \right]^2 \delta_{\mathbf{q}, 0} \\ &\quad + \frac{1}{(2\pi)^2} \sum_{s_1, s_2 = \pm} s_1 s_2 \sum_{\mathbf{k}_1, \mathbf{k}_2} \\ &\quad \times \langle \langle \mathcal{G}^{s_1}(\mathbf{k}_1, \mathbf{k}_1 - \mathbf{q}, \omega) \mathcal{G}^{s_2}(\mathbf{k}_2, \mathbf{k}_2 + \mathbf{q}, \omega) \rangle \rangle, \end{aligned}$$

and $\langle \langle \dots \rangle \rangle$ refers to a disorder-averaging process in which only *connected* diagrams are retained. The first term on the right hand side of this equation corresponds to the disconnected diagram shown in Fig. 3(a), and is also equal to $|\langle \rho(\mathbf{q}, \omega) \rangle|^2$. Thus, the variance of $\rho(\mathbf{q}, \omega)$ is

$$\langle \Delta \rho^2(\mathbf{q}, \omega) \rangle = \frac{-1}{(2\pi)^2} \sum_{s_1, s_2 = \pm} s_1 s_2 I^{s_1 s_2}(\mathbf{q}, \omega) \quad (9)$$

where the disorder-averaged two-particle response kernel $I^{s_1 s_2}(\mathbf{q}, \omega)$ is

$$I = \frac{1}{N^2} \sum_{\mathbf{k}_1, \mathbf{k}_2} \langle \langle \mathcal{G}^{s_1}(\mathbf{k}_1, \mathbf{k}_1 - \mathbf{q}, \omega) \mathcal{G}^{s_2}(\mathbf{k}_2, \mathbf{k}_2 + \mathbf{q}, \omega) \rangle \rangle. \quad (10)$$

We first consider the leading order contribution to the FTDOS, which is shown in Fig. 3(b) and which can be written as

$$\begin{aligned} \langle \Delta \rho_1^2(\mathbf{q}, \omega) \rangle &= N_i \left[\frac{\text{Im}}{\pi N} \sum_{\mathbf{k}} G^+(\mathbf{k}, \omega) T_{\mathbf{k}, \mathbf{k} + \mathbf{q}}^+(\omega) \right. \\ &\quad \left. \times G^+(\mathbf{k} + \mathbf{q}, \omega) \right]^2, \quad (11) \end{aligned}$$

where $T_{\mathbf{k},\mathbf{k}+\mathbf{q}}^+(\omega)$ is the retarded scattering T-matrix describing scattering from a single impurity embedded in a medium with impurity concentration $n_i = N_i/N$. The astute reader will recognize that this appears to simply be the square of single-impurity result (multiplied by N_i) which is widely used to describe the FTDOS in strongly-correlated superconductors.¹⁵ The key difference here is that the Green's functions and T-matrix are now evaluated at the level of the self-consistent T-matrix approximation¹⁶ (SCTMA). This approximation amounts to solving the one-impurity problem in an effective medium characterized by a self-energy $\Sigma(\mathbf{k},\omega)$ which approximately describes the remaining $N_i - 1$ impurities. In this approximation, the self-consistency condition is $\Sigma(\mathbf{k},\omega) = n_i T_{\mathbf{k},\mathbf{k}}(\omega)$, and it can be shown that this is equivalent to the coherent potential approximation in the dilute limit. This result—that the addition of a self-energy to the Green's function accounts for many-impurity effects to leading order—has been taken as an ansatz by several authors,^{17,18} but has not previously been formally justified.

The evaluation of Eq. (11) is simplest in the case of a random distribution of pointlike impurities with scattering potential V_0 . In this case, the T-matrix loses its dependence on \mathbf{k} and \mathbf{q} and we have the following system of equations which must be self-consistently solved:

$$\begin{aligned}\Sigma^\pm(\omega) &= n_i T^\pm(\omega) \\ G^\pm(\mathbf{k},\omega) &= [\omega^\pm - \epsilon_{\mathbf{k}} - \Sigma^\pm(\omega)]^{-1} \\ g^\pm(\omega) &= \frac{1}{N} \sum_{\mathbf{k}} G^\pm(\mathbf{k},\omega) \\ T^\pm(\omega) &= V_0/[1 - V_0 g^\pm(\omega)]\end{aligned}$$

with $\omega^\pm = \omega \pm i\eta$ and η a positive, real, infinitesimal. The results of this calculation are compared with numerical results of the previous section in Fig. 4. In general, the agreement between the leading-order diagrammatic and numerical approaches is good, except for the broad peak centered at $\mathbf{q} = 0$ which is present in the numerical calculations and absent in the leading-order approximation. This peak is distinct from the $\mathbf{q} = 0$ peak in Eq. (2) (which occurs strictly at $\mathbf{q} = 0$ and is $\sim O(N)$) and arises from higher order diagrams. The finite- \mathbf{q} peak heights in the diagrammatic calculations scale as $\sqrt{N_i}$, as shown in Fig. 4(c) and (d), in agreement with the scaling of the numerical results discussed previously. The scattering rate in (d) is approximately twice that in (c), and it is interesting that, apart from the overall scaling of the spectrum, the most significant effect of scattering is to enhance the background. Thus, one's ability to resolve the peaks is not limited by a reduction of their height, but by a reduction in contrast with the background.

In order to get an understanding of the effects of higher order diagrams, we consider the three possible second

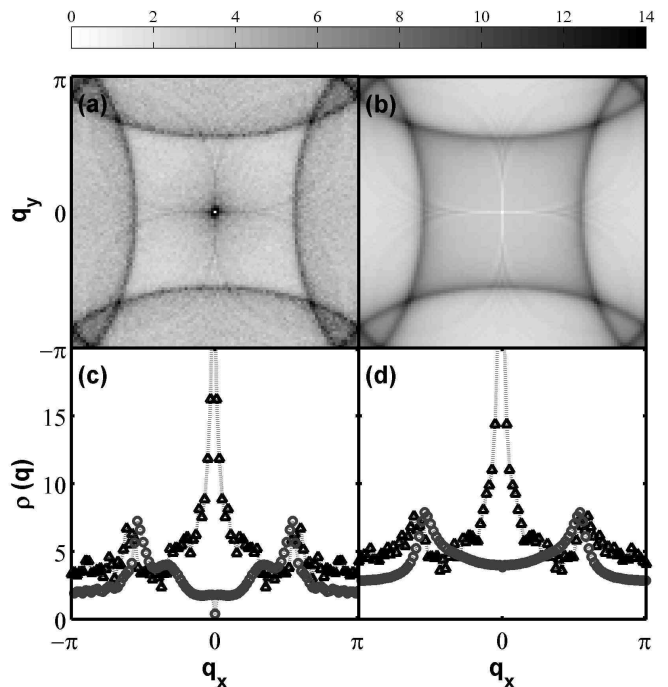


FIG. 4: (color online) Comparison of diagrammatic and numerical $\rho_{\text{rms}}(\mathbf{q},\omega)/\sqrt{N_i}$ at $\omega = 0$. Results are shown for 3% impurities for (a) the numerical method with $N_{\text{cfg}} = 29$, and (b) the leading order diagrammatic result given by Eq. (11). Cuts along the line $\mathbf{q} = (q, 0)$ are shown in (c) and (d) for 3% and 6% disorder respectively for exact (red triangles) and diagrammatic (blue circles) calculations.

order diagrams shown in Fig. 3(c), which combine to give

$$\begin{aligned}I_2^{s_1 s_2}(\mathbf{q}) &= \frac{N_i T^{s_1} T^{s_2}}{N^2} \sum_{\mathbf{k}_1, \mathbf{k}_2} G^{s_1}(\mathbf{k}_1) G^{s_1}(\mathbf{k}_1 - \mathbf{q}) \\ &\quad \times G^{s_2}(\mathbf{k}_2) G^{s_2}(\mathbf{k}_2 + \mathbf{q}) [W^{s_1 s_2}(\mathbf{k}_1 + \mathbf{k}_2) \\ &\quad + W^{s_1 s_2}(\mathbf{k}_1 - \mathbf{k}_2 - \mathbf{q}) + 2W^{s_1 s_1}(\mathbf{q})] \quad (12)\end{aligned}$$

$$W^{s_1 s_2}(\mathbf{p}) = n_i T^{s_1} T^{s_2} \frac{1}{N} \sum_{\mathbf{k}} G^{s_1}(\mathbf{k}) G^{s_2}(\mathbf{k} + \mathbf{p}), \quad (13)$$

where we note that $W^{++}(\mathbf{p}) = W^{--}(\mathbf{p})^*$ and $W^{+-}(\mathbf{p}) = W^{-+}(\mathbf{p})$. Both $W^{++}(\mathbf{p})$ and $W^{+-}(\mathbf{p})$ are shown in Fig. 5 at $\omega = 0$. The term $W^{+-}(\mathbf{p}) \approx 1 - Dp^2/2\gamma$ for small p , where D is the diffusion coefficient of the metal,¹⁹ and is substantially larger than $W^{++}(\mathbf{p})$.

We are interested in the largest contribution from the second order diagrams, which comes from the retarded-advanced (W^{+-}) channel. Because $W^{+-}(\mathbf{p})$ is peaked at $\mathbf{p} = 0$, we can evaluate Eq. (9) approximately as:

$$\begin{aligned}\langle \Delta \rho_2^2(\mathbf{q},\omega) \rangle &= \langle \Delta \rho_1^2(\mathbf{q},\omega) \rangle + \frac{N_i T^+ T^-}{\pi^2 N^2} \sum_{\mathbf{p}} W^{+-}(\mathbf{p}) \\ &\quad \times \sum_{\mathbf{k}} |G^+(\mathbf{k}) G^+(\mathbf{k} + \mathbf{q})|^2. \quad (14)\end{aligned}$$

The results of this calculation are shown in Fig. 5(c).

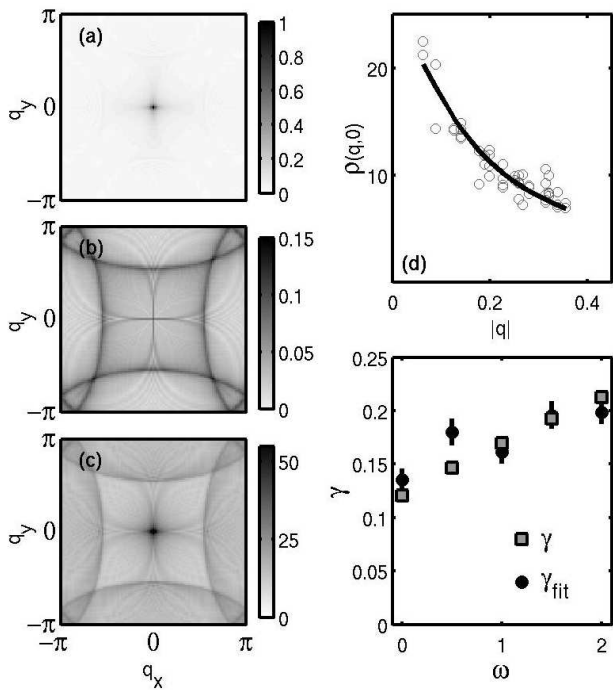


FIG. 5: (color online) Second order corrections to $\rho_{\text{rms}}(\mathbf{q}, \omega)$. Panels (a) and (b) show the vertex functions $W^{+-}(\mathbf{q}, \omega)$ and $W^{++}(\mathbf{q}, \omega)$ respectively from which second order corrections are calculated, (c) shows $\rho_{\text{rms}}(\mathbf{q}, \omega)$ evaluated using Eq. (14); (d) shows a least-squares fit of Eq. (16) to the results of exact numerical calculations at $\omega = 0$; (e) shows the scattering rate γ extracted from the SCTMA self-energy (square) and from fits of Eq.(16) (solid circle) to the $\mathbf{q} = 0$ peak of numerical calculations. Error bars are the standard deviation between the fitted curve and data. Panels (a)-(c) are at $\omega = 0$ and for $n_i = 0.03$, while (d) and (e) are for $n_i = 0.06$ and $N_{\text{cfg}} = 29$.

One sees a weak background structure which is essentially the same as that from the leading order contribution in Eq. (11), but the dominant feature in the second order correction is the central peak. Physically, this suggests that two-impurity processes generally interfere destructively and tend to shift weight to small values of \mathbf{q} . At this level of approximation, however, we do not capture the physics of trapped states, which have been predicted to occur in d-wave superconductors between pairs of impurities satisfying an appropriate resonance criterion.²⁰ Such resonances would tend to enhance finite- \mathbf{q} peaks in the FTDOS.

We note that, while Fig. 5(c) has the same qualitative structure as the exact numerical results shown in Fig. (4), the quantitative agreement is still poor. This is because, in the absence of inelastic dephasing or coupling to the third dimension, weak localization physics affects the FTDOS. One can attempt to go beyond second order in the perturbation series, and the natural step to take is to sum either the ladder or maximally crossed diagrams.

Both of these calculations give the same result:

$$\langle \Delta \rho^2(\mathbf{q}, \omega) \rangle \sim \sum_{\mathbf{p}} \frac{1}{Dp^2} \sum_{\mathbf{k}} |G^+(\mathbf{k})G^+(\mathbf{k} + \mathbf{q})|^2.$$

In 2D, the sum over \mathbf{p} diverges logarithmically, but the divergence will be cut off either by inelastic dephasing or by tunneling out of the surface states.¹⁹ What is perhaps most interesting about this result, however, is the \mathbf{q} -space structure of the central peak, which is the same as in Eq. (14).

We can estimate the form of the central peak in $\langle \Delta \rho^2(\mathbf{q}, \omega) \rangle$ in the limit $q^2/2m \ll v_F q$, where for an isotropic Fermi surface:

$$\frac{1}{N} \sum_{\mathbf{k}} |G^+(\mathbf{k})G^+(\mathbf{k} + \mathbf{q})|^2 = \frac{\pi N_0}{\gamma^2} \frac{1}{\sqrt{(v_F q)^2 + (2\gamma)^2}}, \quad (15)$$

such that, for small \mathbf{q} ,

$$\langle \Delta \rho^2(\mathbf{q}, \omega) \rangle = \frac{A}{\sqrt{1 + (q\ell/2)^2}} \quad (16)$$

where $\ell = v_F/\gamma$ is the mean-free path and A dictates the peak weight. This result suggests that one can extract ℓ from FTSTS experiments. As a check, we have made least-squares fits of Eq. (16) to the central peak of an exact numerical calculation of the type outlined in Sec. IIB with $n_i = 0.06$ and $N_{\text{cfg}} = 29$. We have treated both A and ℓ as fitting parameters, and an example of the numerical data and fitted curve shown in Fig. 5(d) illustrates that Eq. (16) appears to describe the exact result rather well. In Fig. 5(e), the scattering rate $\gamma = v_F/\ell$ extracted from the fitting procedure is shown as a function of ω . For comparison the scattering rate $\gamma = -\text{Im} \Sigma^+(\omega)$ calculated using the SCTMA is also shown. Because the band structure is anisotropic, we have chosen to fit $\rho(\mathbf{q}, \omega)$ as a function of the radial coordinate $q = |\mathbf{q}|$ (note that the point at $\mathbf{q} = 0$ must be excluded), as shown in Fig. 5(d). The fit is therefore to an angular average of the data, and the error bars in Fig. 5(e) are the root-mean-square deviation between the fit and the data. We have experimented with fitting to cuts through the data along various directions, for example $\mathbf{q} = (q, 0)$ and $\mathbf{q} = (q, q)$, but have generally found this to be less reliable than fitting to the angular average. In general, since we are attempting to fit a peak of half-width $\approx 2\ell^{-1}$, a reliable fit requires a \mathbf{q} -space resolution $\Delta q \lesssim 2\ell^{-1}$, or (equivalently) that the region over which one makes the LDOS map is larger than roughly twice the mean-free-path. With these caveats in mind, the good agreement between the self-consistent T-matrix and exact numerical results is heartening, and shows that one can legitimately hope to extract the mean-free path from experiments.

Throughout this work, we have presumed that one is averaging distinct samples. However, for experimental purposes, it may be more straightforward to measure a single large surface area (of side L), and partition the

data into n^2 subregions of side L/n . The benefits of this procedure are that one gains a factor of n in the signal-to-noise ratio, but the cost is a loss of q -space resolution by the same factor n . Provided $L/n \gtrsim \ell$, however, one is not losing important information as a result of the partitioning process.

We finish this section with a brief discussion of inelastic scattering. The essential point is that, since the correlation function measured by $\Delta\rho^2(\mathbf{q}, \omega)$ is between single-particle Green's functions, and is not a two-particle correlation function, there are no "vertex-correction" diagrams in which inelastic propagators connect the upper and lower Green's functions in Fig. 3. To put it another way, unless one has localized bosonic modes attached to the impurity sites, inelastic scattering will be spatially uniform and will not produce Friedel oscillations. Such Friedel oscillations would be described by inelastic vertex-correction diagrams, and thus these diagrams must be absent. The effect of inelastic scattering is, therefore, solely to modify the single-particle self-energy. Since it is the total scattering rate which determines peak heights and widths in $\Delta\rho^2(\mathbf{q}, \omega)$, separation

of elastic and inelastic scattering rates is difficult. In particular, the scattering rate one extracts from Eq. (16) contains both the elastic and inelastic scattering rates.

III. SUMMARY

We have studied the disorder-averaged variance $\langle\Delta\rho^2(\mathbf{q}, \omega)\rangle$ of the density of states of a disordered 2D metallic surface. Through a combination of numerical and analytic calculations, we have shown that disorder-averaging is an effective means of increasing the signal-to-noise ratio in the Fourier transformed local density of states. This resolves a problem with the conventional experimental technique of measuring $\rho(\mathbf{q}, \omega)$ for which the signal-to-noise ratio remains fixed as one averages over impurity configurations. Furthermore, we have shown that one can construct a diagrammatic perturbation theory for $\langle\Delta\rho^2(\mathbf{q}, \omega)\rangle$ and that it is possible to extract an important physical property, the mean-free-path, from the central peak in the FTSTS spectrum.

-
- ¹ P. T. Sprunger, L. Petersen, E. W. Plummer, E. Laegsgaard, and F. Besenbacher, *Science* **275**, 1764 (1997)
- ² L. Petersen, P. T. Sprunger, Ph. Hofmann, E. Laegsgaard, B. G. Briner, M. Doering, H.-P. Rust, A. M. Bradshaw, F. Besenbacher, and E. W. Plummer, *Phys. Rev. B* **57**, R6858 (1998); L. Petersen, P. Laitenberger, E. Laegsgaard, and F. Besenbacher, *Phys. Rev. B* **58**, 7361 (1998).
- ³ K. Hojrup Hansen, J. Gottschalk, L. Petersen, B. Hammer, E. Laegsgaard, F. Besenbacher, and I. Stensgaard, *Phys. Rev. B* **63** 115421(2001).
- ⁴ M. Morgenstern, J. Klijn, Chr. Meyer, M. Getzlaff, R. Adelung, R. A. Römer, K. Rossnagel, L. Kipp, M. Skibowski, and R. Wiesendanger, *Phys. Rev. Lett.* **89**, 136806 (2002).
- ⁵ P. Ruffieux, M. Melle-Franco, O. Gröning, M. Biemann, F. Zerbetto, and P. Gröning, *Phys. Rev. B* **71**, 153403 (2005).
- ⁶ F. Vonau, D. Aubel, G. Gewinner, C. Pirri, J. C. Peruchetti, D. Bolmont, and L. Simon, *Phys. Rev. B* **69**, 081305R (2004).
- ⁷ J. E. Hoffman, K. McElroy, D.-H. Lee, K. M. Lang, H. Eisaki, S. Uchida, and J. C. Davis, *Science* **297**, 1148 (2002); K. McElroy, R. W. Simmonds, J. E. Hoffman, D.-H. Lee, J. Orenstein, H. Eisaki, S. Uchida, and J. C. Davis, *Nature* **422**, 592 (2003);
- ⁸ C. Howald, H. Eisaki, N. Kaneko, M. Greven, and A. Kapitulnik, *Phys. Rev. B* **67**, 014533 (2003)
- ⁹ Michael Vershinin, Shashank Misra, S. Onon, Y. Abe, Yoichi Ando, and Ali Yazdani, *Science* **303**, 5666 (2004).
- ¹⁰ T. Hanaguri, C. Lupien, Y. Kohsaka, D.-H. Lee, M. Azuma, M. Takano, H. Takagi, and J. C. Davis, *Nature* **430**, 1001 (2004).
- ¹¹ J.-X. Zhu, J. Sun, Q. Si, and A. V. Balatsky, *Phys. Rev. Lett.* **92**, 017002 (2004); Jinn-Xin Zhu, A. V. Balatsky, T. P. Devereaux, Qimiao Si, J. Lee, K. McElroy, and J. C. Davis, cond-mat/0507610 (unpublished).
- ¹² L. Capriotti, D. J. Scalapino, and R. D. Sedgewick, *Phys. Rev. B* **68**, 014508 (2003).
- ¹³ Lingyin Zhu, W. A. Atkinson, and P. J. Hirschfeld, *Phys. Rev. B* **69**, 060503 (2004).
- ¹⁴ One can solve directly for the many-impurity T-matrix as in Ref. 13.
- ¹⁵ Qiang-Hua Wang and Dung-Hai Lee, *Phys. Rev. B* **67**, 020511 (2003).
- ¹⁶ E. N. Economou, *Green's Functions in Quantum Physics* (Springer-Verlag, New York, 1983); W. A. Atkinson, P. J. Hirschfeld, and A. H. MacDonald, *Phys. Rev. Lett.* **85**, 3922 (2000).
- ¹⁷ R. S. Markiewicz, *Phys. Rev. B* **69**, 214517 (2004).
- ¹⁸ S. Misra, M. Vershinin, P. Phillips, and A. Yazdani, *Phys. Rev. B* **70**, 220503 (2004).
- ¹⁹ B. L. Altshuler and A. G. Aronov, in *Electron-Electron Interactions in Disordered Systems*, edited by A. L. Efros and M. Pollak (North-Holland, New York 1985).
- ²⁰ L. Zhu, W. A. Atkinson, and P. J. Hirschfeld, *Phys. Rev. B* **67**, 094508 (2003); D. K. Morr and N. A. Stavropoulos, *Phys. Rev. B* **66**, 140508 (2002).